Dalton Transactions

RSC Publishing

PAPER

View Article Online
View Journal | View Issue

Cite this: *Dalton Trans.*, 2013, **42**, 12452

Synthesis, spectral and redox switchable cubic NLO properties of chiral dinuclear iron cyanide/isocyanide-bridged complexes†

Xiao Ma,[a] Chen-Sheng Lin,[a] Hui Zhang,[b] Yi-Ji Lin,[b] Sheng-Min Hu,[a] Tian-Lu Sheng*[a] and Xin-Tao Wu[a]

Received 7th May 2013,
Accepted 29th June 2013

DOI: 10.1039/c3dt51197a

www.rsc.org/dalton

Two chiral dinuclear cyanide/isocyanide-bridged complexes (*R*)-[Cp(dppe)Fe–CN–Fe(dppp)Cp]PF_6 (**1**[PF_6]) and (*R*)-[Cp(dppe)Fe–NC–Fe(dppp)Cp]PF_6 (**2**[PF_6]), and their mono-oxidation products (*R*)-[Cp(dppe)Fe^{II}–CN–Fe^{III}(dppp)Cp] [PF_6]$_2$ (**1**[PF_6]$_2$) and (*R*)-[Cp(dppe)Fe^{III}–NC–Fe^{II}(dppp)Cp][PF_6]$_2$ (**2**[PF_6]$_2$) were synthesized and fully characterized. The electronic spectra of both the mixed-valence complexes **1**[PF_6]$_2$ and **2**[PF_6]$_2$ exhibit a strong and broad absorption band with two discernable peaks in the NIR region, which are attributed to Fe(II)–Fe(III) IVCT transitions. The attributions are supported by the DFT calculations. Under irradiation with a nanosecond laser at 1064 nm, the measured third-order NLO results of all four cyanide-bridged complexes showed that complexes $\mathbf{1}^{+}$ and $\mathbf{2}^{+}$ do not exhibit an NLO response, but their one-electron oxidation complexes $\mathbf{1}^{2+}$ and $\mathbf{2}^{2+}$ exhibit a strong NLO response due to a resonance enhanced effect. In addition, both complexes $\mathbf{1}^{2+}$ and $\mathbf{2}^{2+}$ display RSA and self-defocusing effects and show good optical limiting behavior in a broadband range.

Introduction

The nonlinear optical (NLO) properties of molecular materials have attracted considerable attention due to their applications in data storage, telecommunications, image processing, optical limiting and switching materials.[1] In the field of nonlinear optics, organometallic complexes compared to inorganic complexes possess some advantages such as large NLO responses, fast response times, good design flexibility and switchable properties. To pursue the relationship between molecular structure and NLO properties in this field, large numbers of organometallic complexes with good NLO properties have been synthesized and studied over the past thirty years.[1,2] In particular, organometallic mixed-valence complexes, usually containing low-energy absorption bands in the Vis-NIR region, exhibit similar properties to organic donor–acceptor molecules, which could present a good NLO response.[3,4] In 1993, Laidlaw and co-workers studied the second-order response of two cyanide-bridged organometallic mixed-valence complexes by the hyper-Rayleigh scattering technique, and found that those complexes show a large first hyperpolarizability, which is attributed to the intervalence charge-transfer (IVCT) states in the mixed-valence complexes and the near-resonant enhancement caused by the proximity of the input laser beam and IVCT transition frequencies.[3] Moreover, the third-order NLO properties of the mixed-valence complexes with low-lying excited state energy have also been largely studied by Mark G. Humphrey and co-workers.[5,6] Likewise, those studies revealed that the low-lying energy transitions, such as the IVCT of the mixed-valence complexes, play an important role in the third-order NLO response.[5,7] Therefore, it would be expected that large NLO response materials can be obtained by modifying the intensity and position of the IVCT transition of mixed-valence complexes.

For many years, studies of cyanide-bridged mixed-valence complexes have been mainly devoted to the electron transfer process[8] and magnetism.[9] In contrast, the NLO properties of such complexes have been rarely reported. Recently, an important topic in the nonlinear field is to study the combination of third-order optical nonlinearity with chirality, which can not only further broaden our knowledge about light–matter interaction, but also produce many practical applications in

[a]*State Key Laboratory of Structural Chemistry, Fujian Institute of Research on the Structure of Matter, Chinese Academy of Sciences, Fuzhou, Fujian 350002, China. E-mail: tsheng@fjirsm.ac.cn*

[b]*State Key Laboratory of Physical Chemistry of Solid Surface and Department of Chemistry, College of Chemistry and Chemical Engineering, Xiamen University, Xiamen 361005, China*

†Electronic supplementary information (ESI) available: Cyclic voltammogram, the calculated orbital diagrams and *Z*-scan measurements for $\mathbf{2}^{+}$; the solvent dependence of IVCT bands for $\mathbf{1}^{2+}$ and $\mathbf{2}^{2+}$; crystallographic data and structure refinements summary for complexes $\mathbf{1}^{+}$ and $\mathbf{2}^{+}$. CCDC 937175 and 937176 for $\mathbf{1}^{+}$ and $\mathbf{2}^{+}$. For ESI and crystallographic data in CIF or other electronic format see DOI: 10.1039/c3dt51197a

several fields of science and technology.[10] Our research interest mainly focuses on the study of third-order nonlinearity of mixed-valence chiral complexes. In this work, a dinuclear chiral cyanide-bridged complex (*R*)-[Cp(dppe)Fe–CN–Fe(dppp)-Cp]PF_6 (**1**[PF_6]) and its mono-electron oxidation product (*R*)-[Cp(dppe)Fe–CN–FeCp(dppp)][PF_6]$_2$ (**1**[PF_6]$_2$) were synthesized and characterized. For comparison, the cyanide-inversed complexes of **1**[PF_6] and **1**[PF_6]$_2$, namely (*R*)-[Cp(dppe)Fe–NC–Fe-(dppp)Cp]PF_6 (**2**[PF_6]) and (*R*)-[Cp(dppe)Fe–NC–FeCp(dppp)]-[PF_6]$_2$ (**2**[PF_6]$_2$) (dppe = bis(diphenylphosphino)-ethane, dppp = (*R*)-(+)-1,2-bis(diphenylphosphino)propane), were also synthesized and characterized. The spectroscopic properties of all four complexes have been studied, and rationalized by density functional theory (DFT) calculation. In addition, the third-order NLO properties of the four complexes have been investigated using *Z*-scan technology. Furthermore, the optical limiting properties of both **1**[PF_6]$_2$ and **2**[PF_6]$_2$ have also been measured.

Results and discussion

Synthesis and structural characterization

The reaction of Cp(dppe)FeCN with Cp(dppp)Fe($NCCH_3$)Br in methanol, followed by addition of NH_4PF_6, gave a red brown chiral dinuclear complex **1**[PF_6] in 82% yield. Similarly, **2**[PF_6] was prepared by the reaction of Cp(dppp)FeCN with Cp(dppe)-Fe($NCCH_3$)Br in 86% yield. Both the complexes were characterized using ESI^+ mass spectra, elemental analysis and single-crystal X-ray structure analysis.

Complexes **1**[PF_6] and **2**[PF_6] crystallize in the triclinic space group *P*1 with two molecules in a unit cell. Fig. 1 shows one of two molecules of both the complexes. For **1**[PF_6], if one considers the centroid of the Cp ring, two iron atoms connected by a cyanide bridge exhibit tetrahedron coordination, in which Fe1 is bonded to dppe and Fe2 bonded to dppp. The bond distances of Fe–C (Cp) vary from 2.025 to 2.151 Å, and the bond distances of Fe–C (CN) (1.881(16)/1.909(15) Å) are comparable to the parent complex Cp(dppe)FeCN (Fe–C (CN) 1.895(5) Å) and the chelated Cp(dppe)Fe(CN) derivatives.[11,12] The Fe–C (CN) (1.881(16)/1.909(15) Å) bonds are slightly shorter than the Fe–N (CN) (1.890(12)/2.048(16) Å). The C≡N bond distance is close to that observed in the literature.[11,13] The bridging array Fe–C≡N–Fe (Fe–C–N 172.0(12)°, Fe–N–C 167.7(13)°) slightly deviates from the linear. As shown in Fig. 1, **2**[PF_6] is almost identical to complex **1**[PF_6] from bond length to bond angle. The Fe1–N1 (CN) (1.928(14) Å) bonds are slightly longer than the Fe1–C1 (CN) (1.883(15) Å) bonds. It should be mentioned that the quality of a single crystal of **2**[PF_6] is relatively poor. Thus, further comparisons are meaningless. However, a marked difference between them is that the cyanide of $\mathbf{2}^+$ is inverse compared to that of $\mathbf{1}^+$, which is also supported by the following spectral properties.

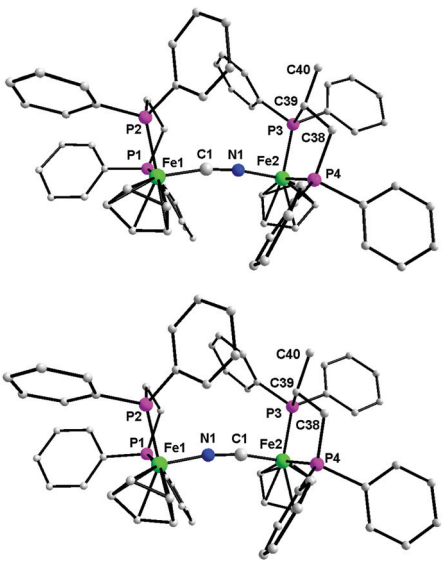

Fig. 1 Molecular structure of $\mathbf{1}^+$ (top) and $\mathbf{2}^+$ (bottom) (hydrogen atoms are omitted for clarity).

Electrochemistry and spectra

Both complexes $\mathbf{1}^+$ and $\mathbf{2}^+$ were subjected to cyclic voltammetry in acetonitrile. As shown in Fig. 2, complex $\mathbf{1}^+$ shows two chemically reversible oxidation waves corresponding to Fe^{II}–CN–Fe^{II}/Fe^{II}–CN–Fe^{III} (0.20 V *vs.* Ag/AgCl) and Fe^{II}–CN–Fe^{III}/Fe^{III}–CN–Fe^{III} (0.88 V *vs.* Ag/AgCl). For $\mathbf{2}^+$, the reversible oxidation potentials corresponding to Fe^{II}–NC–Fe^{II}/Fe^{III}–NC–Fe^{II} and Fe^{III}–NC–Fe^{II}/Fe^{III}–NC–Fe^{III} are 0.22 and 0.87 V (Fig. S1†), respectively. These suggest the presence of electronic interactions between the two Fe atoms in both the complexes. Based on the electrochemistry data, the reactions of both $\mathbf{1}^+$ and $\mathbf{2}^+$ with 1 equiv. $(Cp)_2FePF_6$ give their mono-oxidation products $\mathbf{1}^{2+}$ and $\mathbf{2}^{2+}$, respectively. The solid salts and their solutions of both the oxidized complexes are stable for a long period of time in air. Both $\mathbf{1}^{2+}$ and $\mathbf{2}^{2+}$ were confirmed by their ESI^+ mass spectra and their elemental analysis data. The EPR spectra of both the mono-oxidation products $\mathbf{1}^{2+}$ and $\mathbf{2}^{2+}$ show the presence of single electron in the room temperature solutions (Fig. S2†). The *g*-factor of both the complexes is about 2.11.

The CN stretching peaks of complexes $\mathbf{1}^{n+}$ and $\mathbf{2}^{n+}$ (n = 1, 2) given in the Experimental section show characteristic stretching frequency. The cyanide band of $\mathbf{1}^+$ (2051 cm^{-1}) slightly shifts to low frequency compared to the parent complex

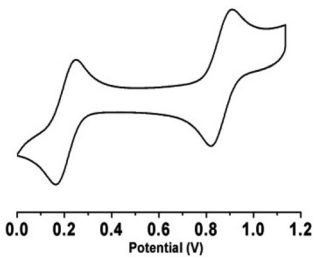

Fig. 2 Cyclic voltammogram of complex $\mathbf{1}^+$ in a 0.10 M acetonitrile solution of Bu_4NPF_6 at a scan rate of 100 mV s^{-1}.

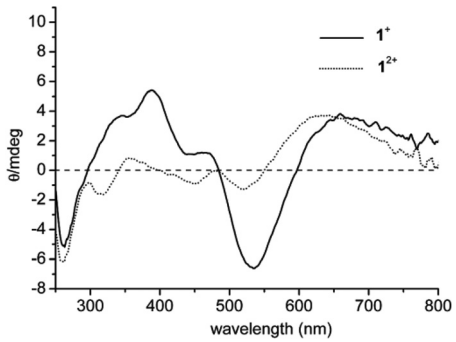

Fig. 3 The solid-state CD spectra of complexes $\mathbf{1}^{+}$ and $\mathbf{1}^{2+}$.

Cp(dppe)FeCN (2062 cm^{-1}), but that of $\mathbf{2}^{+}$ (2062 cm^{-1}) is very close to the parent complex Cp(dppp)FeCN (2064 cm^{-1}). Upon oxidation, the cyanide bands of both $\mathbf{1}^{2+}$ (1991 cm^{-1}) and $\mathbf{2}^{2+}$ (1987 cm^{-1}) distinctly shift to lower frequencies. This can be understood by the π back-bonding effect from the central Fe^{II} into the CN bond which is increased by the withdrawal of charge from the cyanide to Fe^{III}, resulting in the ν(CN) band shifts to a lower frequency.[14]

To confirm the chiral characteristic of complexes $\mathbf{1}^{+}$ and $\mathbf{1}^{2+}$, their solid-state CD spectra from 250 nm to 800 nm were collected by using a KCl pellet (complex/KCl = 1/100) shown in Fig. 3. Complex $\mathbf{1}^{+}$ exhibits two negative CD bands at 260 and 535 nm and two positive Cotton effect signs at 388 nm (with two shoulder peaks centered at 343 and 467 nm) and 660 nm, respectively. Compared to complex $\mathbf{1}^{+}$, the mono-oxidation complex $\mathbf{1}^{2+}$ also displays a negative Cotton signal at 260 nm, but exhibits slightly different Cotton signals between 300 nm and 800 nm, with three weak negative Cotton effects at 318, 450 and 520 nm as well as two positive CD bands at 354 and 627 nm, respectively.

The UV/vis/NIR spectra of complexes $\mathbf{1}^{n+}$ (n = 1, 2) and $\mathbf{2}^{n+}$ (n = 1, 2) were measured in a CH_2Cl_2 solution and are shown in Fig. 4. The absorption band of both complexes $\mathbf{1}^{+}$ and $\mathbf{2}^{+}$ are very similar, predominantly located in the UV-vis region. Differently and significantly, their mono-oxidation products exhibit a new and very broad absorption band containing two discernable peaks (896 and 1090 nm for $\mathbf{1}^{2+}$, 905 and 1112 nm for $\mathbf{2}^{2+}$) in the NIR region, which can be attributed to Fe(II)–Fe(III) IVCT. It is worth mentioning that although the observation of two/three IVCT has been reported in some dinuclear Ru or Os mixed-valence complexes,[15,16] this is relatively rare for dinuclear iron mixed-valence complexes.[17] This is mainly attributed to the decreased magnitudes of the spin–orbit coupling for the Fe d^5–d^6 system; as a result, closely spaced IVCT bands are overlapped.[16] Moreover, the solvent dependences of IVCT bands of complexes $\mathbf{1}^{2+}$ and $\mathbf{2}^{2+}$ were recorded and are shown in Fig. S3–S4.† Both IVCT bands are slightly different from peak strength to peak position in the different solvents. Interestingly, in CH_3OH, the first IVCT peak strength of $\mathbf{1}^{2+}$ is higher than the second one, whereas the first IVCT peak strength of $\mathbf{2}^{2+}$ is lower than the second one. Approximately, the peak shape of IVCT bands of $\mathbf{1}^{2+}$ and $\mathbf{2}^{2+}$ is mirror

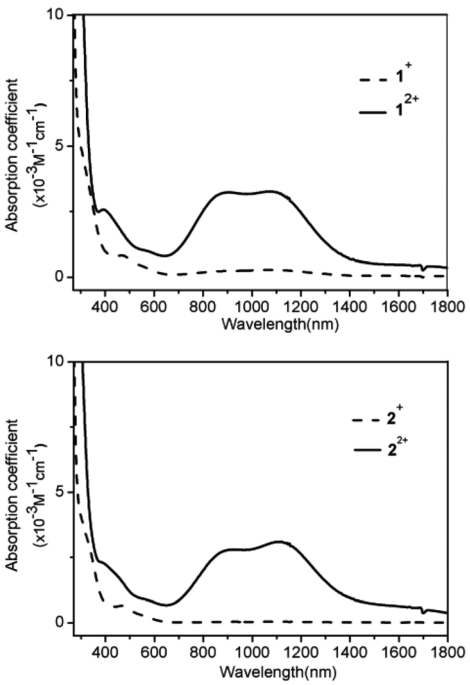

Fig. 4 UV/vis/NIR spectra of complexes $\mathbf{1}^{n+}$ and $\mathbf{2}^{n+}$ (n = 1, 2) in CH_2Cl_2.

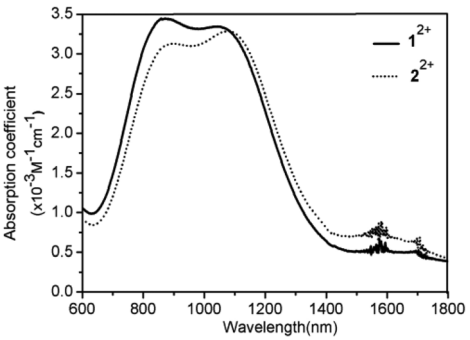

Fig. 5 IVCT bands of complexes $\mathbf{1}^{2+}$ and $\mathbf{2}^{2+}$ in CH_3OH.

symmetry when one neglects the slightly different strength of both complexes (Fig. 5). This interesting phenomenon might arise from the solvent effect and the nature of the complexes.

To interpret the spectroscopic features, TD-DFT calculations were performed without consideration of the solvent effect by the optimized geometries of $\mathbf{1}^{2+}$ and $\mathbf{2}^{2+}$ in which phenyl was substituted by hydrogen at the level of B3LYP/LanL2DZ for Fe and 6-31G* for other atoms. The HOMO and LUMO diagrams of $\mathbf{1}^{2+}$ and frontier orbital diagrams of its two predicted excited states are shown in Fig. 6a–d, respectively. These diagrams of $\mathbf{2}^{2+}$ are provided in the ESI (Fig. S5†). For $\mathbf{1}^{2+}$, Fig. 6c shows the electron flowing at the excitation of 1.323 eV (937 nm), and Fig. 6d corresponds to the excitation of 1.075 eV (1152 nm). Similarly, $\mathbf{2}^{2+}$ has the same excited state energy. Based on the orbital analysis, both transitions could be attributed to Fe(II)–Fe(III) IVCT, which is in very good accord with the experimental absorption spectra. Unfortunately, we failed to explain the

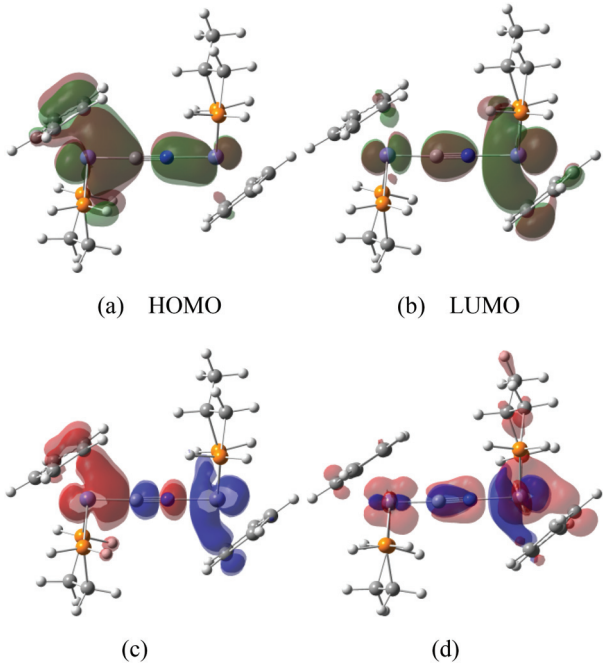

Fig. 6 Molecular orbital diagrams of HOMO (a) and LUMO (b) of $\mathbf{1}^{2+}$; the isosurface value is ±0.02 e Å^{-3}; (c) and (d) are the deformation of charge densities of $\mathbf{1}^{2+}$ in the predicted 1.323 and 1.075 eV excitations, respectively. The blue surfaces indicate regions that have gained the charge with respect to the ground state, and the red surfaces indicate the charge depletion. The isosurface value is ±0.001 e Å^{-3}.

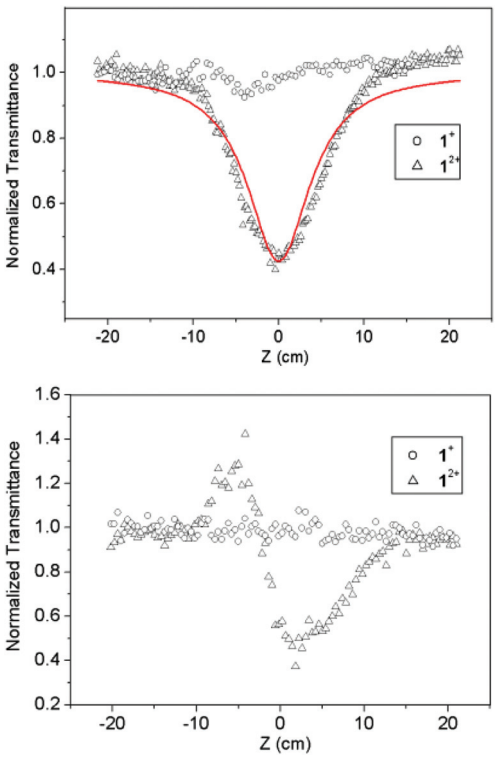

Fig. 7 Open aperture *Z*-scan (the nonlinear absorptive) traces and closed aperture *Z*-scan (the nonlinear refractive index) traces for $\mathbf{1}^{n+}$ (n = 1, 2) in CH_2Cl_2.

difference of IVCT bands of $\mathbf{1}^{2+}$ and $\mathbf{2}^{2+}$ in CH_3OH by the calculation even when considering the solvent effect.

NLO properties

The change of linear absorption is usually concomitant with a change of the NLO property, and then the third-order NLO properties of all four complexes were investigated by the *Z*-scan method at 1064 nm. Their nonlinear absorptions and nonlinear refractions can be separately measured with open-aperture (OA) and closed-aperture (CA) *Z*-scan experiments. OA and CA figures of complexes $\mathbf{1}^{n+}$ (n = 1, 2) are shown in Fig. 7a and 7b, respectively. In Fig. 7a, OA figure of $\mathbf{1}^{+}$ is almost linear, suggesting its negligible nonlinear absorption under the present experimental conditions, but its mono-oxidation product $\mathbf{1}^{2+}$ clearly exhibits a minimum close to the waist, revealing a reverse saturable absorption (RSA) with a positive nonlinear absorption coefficient β. In Fig. 7b, the linear CA figure of $\mathbf{1}^{+}$ displays the absence of nonlinear refraction, while the valley–peak pattern of the CA curve of $\mathbf{1}^{2+}$ indicates that its refractive index is negative, exhibiting a self-defocusing effect. OA and CA figures of complex $\mathbf{2}^{n+}$ (n = 1, 2) are shown in Fig. S6,† respectively. As expected, complex $\mathbf{2}^{+}$ similar to complex $\mathbf{1}^{+}$ does not exhibit the observable nonlinear absorption or nonlinear refractive effect, and complex $\mathbf{2}^{2+}$ similar to complex $\mathbf{1}^{2+}$ also belongs to a reverse saturable absorber with a positive nonlinear absorption coefficient. At the same time, complex $\mathbf{2}^{2+}$ possesses a negative nonlinear refractive index, exhibiting a self-defocusing effect. The NLO absorptive experimental data can be represented by eqn (1), and the effective third-order nonlinear refractive coefficient n_2 can be derived from the difference between the normalized transmittance values at the valley and peak positions ΔT_{v-p} using eqn (2).[18]

$$T_{OA} = \sum_{m=0}^{\infty} \frac{\left[-\frac{\beta I_0 L_{eff}}{1+\frac{z^2}{z_0^2}}\right]^m}{(m+1)^{3/2}} \quad (1)$$

$$n_2 = \frac{\lambda}{0.790\pi\, I_0 L_{eff}} \Delta T_{v-p} \quad (2)$$

where T_{OA} is the normalized transmittance for OA, β is the nonlinear absorption coefficient, $L_{eff} = [1 - \exp(-\alpha_0 L)]/\alpha_0$ is the effective thickness of the sample (L is its thickness) in which α_0 is the linear absorption coefficient, λ is the laser wavelength, I_0 is the on-axis irradiance at the focus, z is the distance of the sample from the focus, and z_0 is the Rayleigh length. From these data, the obtained third-order nonlinear absorption coefficient β and the nonlinear refraction coefficient n_2 for complex $\mathbf{1}^{2+}$ are 2.3×10^{-9} cm W^{-1} and -1.25×10^{-13} cm^2 W^{-1}, respectively. As expected, those of complex $\mathbf{2}^{2+}$ (β is 2.2×10^{-9} cm W^{-1}, n_2 is -1.25×10^{-13} cm^2 W^{-1}) are respectively very close to those of complex $\mathbf{1}^{2+}$. The second-order hyperpolarizability γ values for $\mathbf{1}^{2+}$ and $\mathbf{2}^{2+}$ are found to be 1.05×10^{-32} esu ($\mathbf{1}^{2+}$) and 1.04×10^{-32} esu ($\mathbf{2}^{2+}$). Clearly, the large positive β value shows that both complexes $\mathbf{1}^{2+}$ and $\mathbf{2}^{2+}$ exhibit a strong RSA, which should have mainly resulted from the moderately

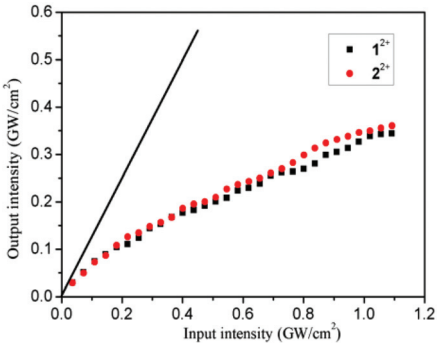

Fig. 8 Optical-limiting behavior of complexes $\mathbf{1}^{2+}$ (circles) and $\mathbf{2}^{2+}$ (square); the straight line represents the linear transmission (80%) of the sample.

strong linear absorption at 1064 nm in the NIR region, related to not only the singlet excited states but also the triplet excited state for the nanosecond pulse duration.[19] On the whole, it can also be seen that both the complexes exhibit a strong nonlinear response, which is mainly due to the near-resonant enhancement caused by the fact that the input laser beam is located in the IVCT transition of the complexes.[20] In addition, based on the above analysis of the very broad NIR absorption band and the strong nonlinear effect of both the mixed-valence complexes, it can be anticipated that both can exhibit a strong nonlinear response in a wide range from 700 nm to 1400 nm because of the resonance enhanced effect. Under irradiation with a 1064 nm laser beam, on the other hand, the distinct nonlinear change from no nonlinear response of $\mathbf{1}^{+}$ and $\mathbf{2}^{+}$ to a strong nonlinear response of $\mathbf{1}^{2+}$ and $\mathbf{2}^{2+}$ makes them possible to be nonlinear switching. That is, $\mathbf{1}^{+}$ and $\mathbf{2}^{+}$ are nonlinearity "off", and $\mathbf{1}^{2+}$ and $\mathbf{2}^{2+}$ are nonlinearity "on".

Generally, the optical limiting behavior of the NLO materials is largely affected by their NLO absorptive and refractive effects. Based on the large NLO absorptive and refractive effects of complexes $\mathbf{1}^{2+}$ and $\mathbf{2}^{2+}$, both optical limiting effects were measured under nanosecond laser pulse, as shown in Fig. 8. It can be found that the optical limiting behaviors of $\mathbf{1}^{2+}$ and $\mathbf{2}^{2+}$ are nearly identical. At very low fluences, they respond linearly to the incident light. When the incident light fluence increases, a deviation from the linear response takes place. The materials become increasingly less transparent as the light fluence rises. Importantly, it can be concluded that both complexes $\mathbf{1}^{2+}$ and $\mathbf{2}^{2+}$ could exhibit optical limiting properties in a very broadband range, which can result from their broad NIR absorption bands.

Conclusions

Two chiral dinuclear cyanide/isocyanide-bridged complexes (*R*)-[Cp(dppe)Fe–CN–Fe(dppp)Cp]PF_6 (**1**[PF_6]), (*R*)-[Cp(dppe)-Fe–NC–Fe(dppp)Cp]PF_6 (**2**[PF_6]) and their mono-oxidation products (*R*)-[Cp(dppe)Fe^{II}–CN–Fe^{III}(dppp)Cp][PF_6]$_2$ (**1**[PF_6]$_2$), (*R*)-[Cp(dppe)Fe^{III}–NC–Fe^{II}(dppp)Cp][PF_6]$_2$ (**2**[PF_6]$_2$) were synthesized and fully characterized. Compared to **1**[PF_6] and **2**[PF_6], both the mixed-valence complexes **1**[PF_6]$_2$ and **2**[PF_6]$_2$ exhibit a strong and broad absorption band with two discernable peaks in the NIR region, which could be attributed to Fe(II)–Fe(III) IVCT transitions. The attributions are supported by the DFT calculation. The measured NLO results of all four cyanide-bridged complexes displayed that, under irradiation with a nanosecond laser at 1064 nm, complexes $\mathbf{1}^{+}$ and $\mathbf{2}^{+}$ do not exhibit an NLO response, but complexes $\mathbf{1}^{2+}$ and $\mathbf{2}^{2+}$ exhibit a strong NLO response. Thus, the effect observed at 1064 nm constitutes the redox cubic NLO switching between two states (nonlinearity "off" and "on"). In addition, both complexes $\mathbf{1}^{2+}$ and $\mathbf{2}^{2+}$ display RSA and self-defocusing effects. Furthermore, it can be anticipated that they could exhibit a strong NLO response and an optical limiting ability in a very broadband range. Much work is ongoing to synthesize a multinuclear mixed-valence cyanide-bridged complex with various low-energy IVCT bands covering a broad wavelength range and to investigate their third-order NLO properties.

Experimental section

General procedures

All manipulations were performed under a nitrogen atmosphere with the use of standard Schlenk techniques unless otherwise stated. All chemicals were reagent grade and used without further purification. Dichloromethane, diethylether and acetonitrile were dried by distilling over calcium hydride under a nitrogen atmosphere. Methanol was dried by distilling over magnesium. Cp(dppe)Fe($NCCH_3$)Br (dppe = bis(diphenylphosphino)ethane), Cp(dppp)Fe($NCCH_3$)Br (dppp = (*R*)-(+)-1,2-bis(diphenylphosphino)-propane), and Cp(dppe)FeCN and Cp(dppp)FeCN were prepared according to the published procedures.[21] Elemental analyses (C, H, N) were carried out on a Vario MICRO elemental analyzer. Infrared (IR) spectra were recorded using a PerkinElmer Spectrum One spectrophotometer with KBr pellets. Solid state CD spectra were recorded using a JASCO J-810 spectropolarimeter. The samples were ground to fine powders with potassium chloride and compressed into transparent disks and the concentration of the complexes was 1.0 wt%. UV-vis-NIR absorption spectra were measured using a Perkin-Elmer Lambda35 UV-vis spectrophotometer. Electrochemical measurements were performed under an argon atmosphere using V3-Studio in an acetonitrile solution containing 0.1 M (Bu_4N)PF_6 as a supporting electrolyte at a scan rate of 100 mV s^{-1}. Glassy graphite and platinum were used as working and counter electrodes, respectively. The potentials were measured against a Ag/AgCl reference electrode. Ferrocene was used as an internal standard. EPR spectra were recorded on the acetonitrile solutions of the complexes at room temperature with a Bruker ELEXSYS E500 spectrometer.

Synthesis of complex $\mathbf{1}^{+}$. To the solution of Cp(dppe)FeCN (54.5 mg, 0.1 mmol) in 10 ml CH_3OH was added Cp(dppp)Fe($NCCH_3$)Br (65.4 mg, 0.1 mmol) under a nitrogen atmosphere, then the reaction mixture was heated to 50 °C and stirred for 12 h, resulting in a colour change from red brown to black brown, and then NH_4PF_6 (50.0 mg) was added to the above

reaction solution. Instantly, a pile of deposit appeared, and then the deposit was collected and washed with diethylether (yield 100 mg, 82%). The black brown crystal was obtained by slowly diffusing diethylether into the dichloromethane solution of **1**[PF_6]. Data for **1**[PF_6]: Anal. Cacld for $Fe_2C_{64}H_{60}NP_5F_6$: C 62.82, H 4.94, N 1.14. Found: C 62.40, H 4.73, N 1.12. IR (KBr, cm^{-1}): 2051 (s) (C≡N). UV-Vis-NIR (CH_2Cl_2): λ_{max}, nm (ε, M^{-1} cm^{-1}): 332 (3564). ESI-MS *m*/*z*: 1078.3 $[\mathbf{1}]^+$.

Synthesis of complex $\mathbf{1}^{2+}$. To a 10 ml dichloromethane solution of **1**[PF_6] (60.0 mg, 0.049 mmol) freshly prepared in methanol was added 1 equiv. of $(Cp)_2FePF_6$ (8.0 mg, 0.049 mmol) at room temperature. The solution changed immediately from dark red brown to gray green. The solvent was concentrated to 2 ml under reduced pressure, and then diethylether was added to the solution to deposit the product. The gray green deposit was collected and washed with diethylether (yield 45 mg, 67%), finally recrystallized by diethylether, but no crytals were obtained. Data for **1**$[PF_6]_2$: Anal. Cacld for $Fe_2C_{64}H_{60}NP_6F_{12}$: C 55.16, H 4.78, N 0.98. Found: C 55.51, H 5.07, N 1.03. IR (KBr, cm^{-1}): 1991 (s) (C≡N). UV-Vis-NIR (CH_2Cl_2): λ_{max}, nm (ε, M^{-1} cm^{-1}): 392 (2575), 896 (3214), 1090 (3251). ESI-MS *m*/*z*: 1222.8 $[\mathbf{1} + PF_6]^+$.

Synthesis of complex $\mathbf{2}^+$. The synthesis method of complex $\mathbf{2}^+$ is similar to that of complex $\mathbf{1}^+$. Cp(dppe)Fe($NCCH_3$)Br (64.0 mg, 0.1 mmol) was added to the methanol solution Cp(dppp)FeCN (56.0 mg, 0.1 mmol), then NH_4PF_6 (50.0 mg) was added to the above reaction solution, and the deposit (105 mg, 86%) was collected. The black brown crystal was obtained by slowly diffusing diethylether into the dichloromethane solution of **2**[PF_6]. Data for **2**[PF_6]: Anal. Cacld for $Fe_2C_{64}H_{60}NP_5F_6$: C 62.82, H 4.94, N 1.14. Found: C 62.90, H 5.12, N 1.28. IR (KBr, cm^{-1}): 2062 (s) (C≡N). UV-Vis-NIR (CH_2Cl_2): λ_{max}, nm (ε, M^{-1} cm^{-1}): 330 (3060). ESI-MS *m*/*z*: 1078.3 $[\mathbf{2}]^+$.

Synthesis of complex $\mathbf{2}^{2+}$. The synthesis method of complex $\mathbf{2}^{2+}$ is similar to that of complex $\mathbf{1}^{2+}$. The gray green complex $\mathbf{2}^{2+}$ is obtained in 74% yield. Its crystal structure has not been obtained. Data for **2**$[PF_6]_2$: Anal. Cacld for $Fe_2C_{64}H_{60}NP_6F_{12}$: C 55.16, H 4.78, N 0.98. Found: C 55.51, H 5.07, N 1.03. IR (KBr, cm^{-1}): 1987 (s) (C≡N). UV-Vis-NIR (CH_2Cl_2): λ_{max}, nm (ε, M^{-1} cm^{-1}): 391 (2289), 905 (2792), 1112 (3067). ESI-MS *m*/*z*: 1222.8 $[\mathbf{2} + PF_6]^+$.

X-ray structure determination

The single crystal data of complexes **1**[PF_6] and **2**[PF_6] were collected using a Saturn70-CCD diffractometer equipped with graphite-monochromatic Mo Kα (λ = 0.71073 Å) radiation by using an ω scan mode at 293.2 K. Crystals of the complexes were quickly isolated and mixed with grease to avoid losing the solvent. The structures were solved by direct methods and refined on F^2 by full-matrix least-squares techniques using the SHELX97 program package.[22] All non-hydrogen atoms were refined anisotropically and the hydrogen atoms were generated geometrically. The large solvent accessible voids in the structure of **1**[PF_6] arise from the loss of solvent molecules. The quality of a single crystal of **2**[PF_6] is relatively poor. Details of data collection and refinement are given in Table S1.†

Theoretical calculations

All calculations have been performed with the Gaussian 03 program package. The TD-DFT electronic excitation calculations were performed using the optimized geometries of $\mathbf{1}^{2+}$ and $\mathbf{2}^{2+}$ in which phenyl was substituted by hydrogen at the level of B3LYP/LanL2DZ for Fe and 6-31G* for others atoms.[23]

Third-order nonlinear measurements

The characterization of nonlinear materials was performed by the *Z*-scan technique. In the *Z*-scan technique, a Gaussian beam is focused on to the sample using a lens and the sample is scanned across the focal region of the lens along the beam propagation direction, *z*.[24] The *Z*-scan technique test gives information on the nonlinear absorptive coefficient and the nonlinear refractive index of the compound. The nonlinear absorptive coefficient and the nonlinear refractive index are obtained using the open aperture *Z*-scan and closed aperture *Z*-scan, respectively. The *Z*-scan experiments were performed using a Nd:YAG laser. The pulse duration was about 13 ns. The repletion frequency is 1 Hz. The *Z*-scan system used a focused spot with w_0 = 54 μm at 1064 nm, and this resulted in Rayleigh lengths greater than 8.61 mm. The thickness of the cell is 1 mm, and so the *Z*-scan studies could safely be treated using the thin sample approximation. The intensity of the incident laser beam at the focus of the laser beam (I_0) was 0.878 GW cm^{-2}. The equipment is calibrated with CS_2 before experiments. Under the same experimental conditions, no detectable nonlinear optics response was observed for the pure solvents, so the solvent contributions to the nonlinear effects of the complexes $\mathbf{1}^{2+}$ and $\mathbf{2}^{2+}$ are negligible. All the NLO experiments were carried out using a 4.4×10^{-4} M solution in dry CH_2Cl_2.

Acknowledgements

This work was supported by grants from the 973 Program (2012CB821702), the National Science Foundation of China (21073192, 21173223, and 21233039), and the Science Foundation of State Key Laboratory of Structural Chemistry (20130008).

References

1 S. Bella, C. Dragonetti, M. Pizzotti, D. Roberto, F. Tessore and R. Ugo, *Top. Organomet. Chem.*, 2010, **28**, 1–55; K. A. Green, M. P. Cifuentes, M. Samoc and M. G. Humphrey, *Coord. Chem. Rev.*, 2011, **255**, 2530–2541; G. S. He, L. S. Tan, Q. Zheng and P. N. Prasad, *Chem. Rev.*, 2008, **108**, 1245–1330; M. G. Humphrey, M. P. Cifuentes and M. Samoc, *Top. Organomet. Chem.*, 2010, **28**, 57–73.

2 R. Liu, D. Zhou, A. Azenkeng, Z. Li, Y. Li, K. D. Glusac and W. Sun, *Chem.–Eur. J.*, 2012, **18**, 11440–11448; G. J. Zhou and W. Y. Wong, *Chem. Soc. Rev.*, 2011, **40**, 2541–2566; W. Sun, B. Zhang, Y. Li, T. M. Pritchett, Z. Li and

J. E. Haley, *Chem. Mater.*, 2010, **22**, 6384–6392; B. J. Coe, J. A. Harris, L. A. Jones, B. S. Brunschwig, K. Song, K. Clays, J. Garin, J. Orduna, S. J. Coles and M. B. Hursthouse, *J. Am. Chem. Soc.*, 2005, **127**, 4845–4859; B. J. Coe, J. A. Harris, B. S. Brunschwig, I. Asselberghs, K. Clays, J. Garin and J. Orduna, *J. Am. Chem. Soc.*, 2005, **127**, 13399–13410; C. E. Powell and M. G. Humphrey, *Coord. Chem. Rev.*, 2004, **248**, 725–756; B. J. Coe, S. Houbrechts, I. Asselberghs and A. Persoons, *Angew. Chem., Int. Ed.*, 1999, **38**, 366–369; T. Verbiest, S. Houbrechts, M. Kauranen, K. Clays and A. Persoons, *J. Mater. Chem.*, 1997, **7**, 2175–2189.

3 W. M. Laidlaw, R. G. Denning, T. Verbiest, E. Chauchard and A. Persoons, *Nature*, 1993, **363**, 58–60.

4 G. Puccetti, M. Blanchard-desce, I. Ledoux, J. M. Lehn and J. Zyss, *J. Phys. Chem.*, 1993, **97**, 9385–9391; J. Casado, V. Hernandez, O. K. Kim, J. M. Lehn, J. T. L. Navarrete, S. D. Ledesma, R. P. Ortiz, M. C. R. Delgado, Y. Vida and E. Perez-Inestrosa, *Chem.–Eur. J.*, 2004, **10**, 3805–3816.

5 N. Gauthier, G. Argouarch, F. Paul, L. Toupet, A. Ladjarafi, K. Costuas, J. F. Halet, M. Samoc, M. P. Cifuentes, T. C. Corkery and M. G. Humphrey, *Chem.–Eur. J.*, 2011, **17**, 5561–5577.

6 M. Samoc, N. Gauthier, M. P. Cifuentes, F. Paul, C. Lapinte and M. G. Humphrey, *Angew. Chem., Int. Ed.*, 2006, **45**, 7376–7379.

7 C. E. Powell, M. P. Cifuentes, J. P. Morrall, R. Stranger, M. G. Humphrey, M. Samoc, B. Luther-Davies and G. A. Heath, *J. Am. Chem. Soc.*, 2003, **125**, 602–610; J. P. Morrall, C. E. Powell, R. Stranger, M. P. Cifuentes, M. G. Humphrey and G. A. Heath, *J. Organomet. Chem.*, 2003, **670**, 248–255.

8 D. M. D'Alessandro and F. R. Keene, *Chem. Rev.*, 2006, **106**, 2270–2298; P. V. Bernhardt, F. Bozoglian, B. P. Macpherson and M. Martinez, *Coord. Chem. Rev.*, 2005, **249**, 1902–1916; L. M. Baraldo, P. Forlano, A. R. Parise, L. D. Slep and J. A. Olabe, *Coord. Chem. Rev.*, 2001, **219**, 881–921; H. Vahrenkamp, A. Geiss and G. N. Richardson, *J. Chem. Soc., Dalton Trans.*, 1997, 3643–3651; B. W. Pfennig, M. R. Norris, N. Zimmerman, J. R. Gallagher and A. I. McCloskey, *Inorg. Chim. Acta*, 2009, **362**, 1701–1708; C. N. Tsai, M. M. Allard, R. L. Lord, D. W. Luo, Y. J. Chen, H. B. Schlegel and J. F. Endicott, *Inorg. Chem.*, 2011, **50**, 11965–11977; J. L. Lin, C. N. Tsai, S. Y. Huang, J. F. Endicott, Y. J. Chen and H. Y. Chen, *Inorg. Chem.*, 2011, **50**, 8274–8280.

9 S. Wang, X.-H. Ding, Y.-H. Li and W. Huang, *Coord. Chem. Rev.*, 2012, **256**, 439–464; X. Y. Wang, C. Avendaño and K. R. Dunbar, *Chem. Soc. Rev.*, 2011, **40**, 3213–3238; M. G. Hilfiger, M. M. Chen, T. V. Brinzari, T. M. Nocera, M. Shatruk, D. T. Petasis, J. L. Musfeldt, C. Achim and K. R. Dunbar, *Angew. Chem., Int. Ed.*, 2010, **49**, 1410–1413; C. Avendano, M. G. Hilfiger, A. Prosvirin, C. Sanders, D. Stepien and K. R. Dunbar, *J. Am. Chem. Soc.*, 2010, **132**, 13123–13125; T. Liu, D. P. Dong, S. Kanegawa, S. Kang, O. Sato, Y. Shiota, K. Yoshizawa, S. Hayami, S. Wu, C. He and C. Y. Duan, *Angew. Chem., Int. Ed.*, 2012, **51**, 4367–4370; M. Nihei, Y. Sekine, N. Suganami, K. Nakazawa, A. Nakao, H. Nakao, Y. Murakami and H. Oshio, *J. Am. Chem. Soc.*, 2011, **133**, 3592–3600; M. Nihei, Y. Okamoto, Y. Sekine, N. Hoshino, T. Shiga, I. P. C. Liu and H. Oshio, *Angew. Chem., Int. Ed.*, 2012, **51**, 6361–6364; A. Bleuzen, V. Marvaud, C. Mathoniere, B. Sieklucka and M. Verdaguer, *Inorg. Chem.*, 2009, **48**, 3453–3466.

10 R. W. Boyd, J. E. Sipe and P. W. Milonni, *J. Opt. A Pure Appl. Opt.*, 2004, **6**, S14–S17; P. Fischer and F. Hache, *Chirality*, 2005, **17**, 421–437; P. P. Markowicz, M. Samoc, J. Cerne, P. N. Prasad, A. Pucci and G. Ruggeri, *Opt. Express*, 2004, **12**, 5209–5214.

11 C. Ornelas, C. Gandum, J. Mesquita, J. Rodrigues, M. H. Garcia, N. Lopes, M. P. Robalo, K. Nattinen and K. Rissanen, *Inorg. Chim. Acta*, 2005, **358**, 2482–2488; D. J. Darensbourg, M. J. Adams, J. C. Yarbrough and A. L. Phelps, *Eur. J. Inorg. Chem.*, 2003, 3639–3648.

12 G. N. Richardson, U. Brand and H. Vahrenkamp, *Inorg. Chem.*, 1999, **38**, 3070–3079.

13 L. Y. Zhang, J. L. Chen, L. X. Shi and Z. N. Chen, *Organometallics*, 2002, **21**, 5919–5925.

14 M. A. Watzky, J. F. Endicott, X. Q. Song, Y. B. Lei and A. Macatangay, *Inorg. Chem.*, 1996, **35**, 3463–3473.

15 D. E. Richardson and H. Taube, *J. Am. Chem. Soc.*, 1983, **105**, 40–51; S. Joss, H. Reust and A. Ludi, *J. Am. Chem. Soc.*, 1981, **103**, 981–982; K. D. Demadis, G. A. Neyhart, E. M. Kober, P. S. White and T. J. Meyer, *Inorg. Chem.*, 1999, **38**, 5948–5959; K. D. Demadis, E. S. El-Samanody, G. M. Coia and T. J. Meyer, *J. Am. Chem. Soc.*, 1999, **121**, 535–544.

16 R. C. Rocha, F. N. Rein, H. Jude, A. P. Shreve, J. J. Concepcion and T. J. Meyer, *Angew. Chem., Int. Ed.*, 2008, **47**, 503–506.

17 T. L. Ph. D. Sheng, *Thesis*, Albert-Ludwigs-Universität, Freiburgim Breisgau, Germany, 2002.

18 G. C. Li, Q. Ren, X. Q. Wang, T. B. Li, H. L. Yang, J. W. Chen and J. N. Zhang, *Appl. Phys. A*, 2011, **104**, 1099–1103; T. Geethakrishnan and P. K. Palanisamy, *Opt. Commun.*, 2007, **270**, 424–428; Y. Ji, J. L. Zuo, L. X. Chen, Y. Q. Tian, Y. L. Song, Y. Z. Li and X. Z. You, *J. Phys. Chem. Solids*, 2005, **66**, 207–212; M. Sheikbahae, A. A. Said and E. W. Vanstryland, *Opt. Lett.*, 1989, **14**, 955–957.

19 T. Cassano, R. Tommasi, M. Arca and F. A. Devillanova, *J. Phys.: Condens. Matter*, 2006, **18**, 5279–5290; X. R. Zhu, Z. R. Sun, R. M. Niu, H. P. Zeng, Z. G. Wang, J. P. Lang, Z. Z. Xu and R. X. Li, *J. Appl. Phys.*, 2003, **94**, 4772–4775; J. H. Si, M. Yang, Y. X. Wang, L. Zhang, C. F. Li, D. Y. Wang, S. M. Dong and W. F. Sun, *Appl. Phys. Lett.*, 1994, **64**, 3083–3085.

20 T. Cassano, R. Tommasi, A. P. Meacham and M. D. Ward, *J. Chem. Phys.*, 2005, **122**, 154507; J. Dai, C. Q. Bian, X. Wang, Q. F. Xu, M. Y. Zhou, M. Munakata, M. Maekawa, M. H. Tong, Z. R. Sun and H. P. Zeng, *J. Am. Chem. Soc.*, 2000, **122**, 11007–11008; C. S. Winter, C. A. S. Hill and A. E. Underhill, *Appl. Phys. Lett.*, 1991, **58**, 107; D. H. Auston,

T. K. Gustafson, A. E. Kaplan, P. L. Kelley and Y.-R. Shen, *Appl. Opt.*, 1987, **26**, 231–234.
21 G. J. Baird and S. G. Davies, *J. Organomet. Chem.*, 1984, **262**, 215–221; P. M. Treichel and D. C. Molzahn, *Syn. React. Inorg. Met.Org. Chem.*, 1979, **9**, 21–29.
22 G. M. Sheldrick, *Acta Crystallogr., Sect. A: Fundam. Crystallogr.*, 2008, **64**, 112–122.
23 A. D. Becke, *J. Chem. Phys.*, 1993, **98**, 5648–5652; C. T. Lee, W. T. Yang and R. G. Parr, *Phys. Rev. B: Condens. Matter*, 1988, **37**, 785–789.
24 W. Zhao and P. Palffymuhoray, *Appl. Phys. Lett.*, 1993, **63**, 1613–1615; M. Sheikbahae, A. A. Said, T. H. Wei, D. J. Hagan and E. W. Vanstryland, *IEEE J. Quantum Electron.*, 1990, **26**, 760–769.